# Effect of atmosphere during additive manufacturing on the microstructure of Ti64

## Bachelor thesis

Ignacio Serrano Socorro
Tutor: Pedro Efrén Martín Concepción

# Abstract

This thesis focuses on exploring the impact of reactive atmospheres on the microstructure and phase composition of titanium alloys manufactured through Laser Powder Bed Fusion (LPBF). The study aims to investigate the effects of inert and reactive atmospheres, analyze process parameters' role in sample quality, and identify areas for improvement.

Samples were fabricated using LPBF under inert Ar and reactive Ar-N2 atmospheres. Optical microscopy and X-ray Diffraction (XRD) techniques were employed for microstructure and phase composition analysis. The findings revealed that Alpha martensite was the dominant phase in both atmospheres, while the Beta phase was not detected. Interestingly, titanium nitrides were observed in the samples printed in the reactive atmosphere, adding an intriguing dimension to the study.

The study also examined the influence of process parameters, such as energy density and laser power, on sample quality and defect formation. Increasing the energy density during printing led to a significant reduction in surface defects and improved print quality. However, further investigations are needed to optimize process parameters and enhance defect reduction strategies.

Overall, this thesis provides valuable insights into the effects of reactive atmospheres on the microstructure and phase composition of titanium alloys in LPBF. It highlights the potential of reactive atmospheres in enhancing the quality and performance of additively manufactured titanium components. The study sets the stage for future research and advancements in the field of titanium alloy additive manufacturing.

# Contents

# 1  Introduction

## 1.1  Titanium

Titanium is a chemical element with the symbol Ti and atomic number 22. It is an industrial metal widely used in various applications due to its strength, lightness, and corrosion resistance. This transition metal has a silver-gray color and exhibits remarkable resistance to corrosion, even in marine and chlorinated environments. These properties make titanium highly desirable for a range of industrial applications.

During the second half of the 20th century, titanium experienced widespread usage in various industries, with the aerospace sector leading the way. The innovative use of titanium in the SR-71 Blackbird program during the 1960s gained significant attention and led to its widespread adoption in aerospace applications. The SR-71 Blackbird, a high-speed strategic reconnaissance aircraft, required a material capable of withstanding high temperatures and pressures, and titanium proved to be an ideal choice.

The unique properties of titanium, such as its high strength-to-weight ratio, corrosion resistance, and biocompatibility, contribute to its attractiveness for diverse industrial applications. The strength-to-weight ratio refers to the ability of a material to bear loads relative to its weight. In the case of titanium, this ratio is high, meaning it can withstand substantial loads considering its weight. This characteristic is particularly valuable in weight-critical applications like aerospace.

Another valuable property of titanium is its resistance to corrosion. Corrosion is a natural process that deteriorates materials over time, especially when exposed to moisture and oxygen. However, titanium is highly resistant to corrosion, enabling it to maintain its integrity and functionality for extended periods compared to other metals.

The biocompatibility of titanium is also significant. It can function within living systems without eliciting adverse immune responses. This property has led to its use in medical applications, including orthopedic and dental implants.

The extensive use of titanium in various industries, coupled with ongoing research into its properties and applications, has made it a subject of great interest in the field of materials science. Materials science is an interdisciplinary field that focuses on studying the properties of materials and discovering ways to alter or enhance those properties to meet specific needs or requirements. Scientists and engineers are continuously exploring ways to improve the properties of titanium and expand its applications.

Additionally, titanium is the tenth most abundant element in the Earth's crust and is typically found in minerals such as ilmenite, rutile, and titanite. It is produced by reducing titanium dioxide with reducing agents like carbon or magnesium.

Titanium's resistance to corrosion is attributed to the formation of a protective oxide layer on its surface, shielding it from corrosion caused by water, saltwater, and most chemicals. This property allows for its use in corrosive environments, such as marine applications and chemical processing equipment.

The high melting point of titanium, around 1,668 degrees Celsius (3,034 degrees Fahrenheit), makes it suitable for high-temperature applications like jet engines and other high-performance machinery.

While titanium possesses numerous desirable qualities, its production is costly due to the labor-intensive extraction process and the energy required for refining. Despite the high price, titanium remains highly sought after for industrial applications due to its unique combination of properties.

One of the most widely used titanium alloys is Ti-6Al-4V, often referred to as the "workhorse" of titanium alloys. It accounts for a significant portion of global titanium usage. Titanium alloys are created by mixing pure titanium with other metals or chemical elements, altering their physical properties.[1]

The Ti-6Al-4V alloy, developed in 1954, exhibits superior properties in terms of heat resistance, strength, plasticity, toughness, formability, weldability, corrosion resistance, and biocompatibility. It constitutes a substantial proportion (75-85%) of all titanium alloys consumed. Many other titanium alloys are modifications of the Ti-6Al-4V alloy. Presently, hundreds of titanium alloys have been developed worldwide, with around 20-30 types gaining significant recognition.

## 1.2 Titanium's manufacturing history

The manufacturing of titanium is a complex process that has evolved over the years. Currently, the most commonly used method for titanium production is the Kroll Process, developed in the 1940s by William J. Kroll. This process involves the reduction of titanium tetrachloride ($TiCl_4$) with magnesium (Mg) in an inert environment to produce sponge titanium, which is then processed into titanium ingots.

The Kroll Process is a multi-stage process that begins with the extraction of titanium ore, typically ilmenite ($FeTiO_3$) or rutile ($TiO_2$), from the earth. This ore is processed to produce $TiCl_4$, which is then reduced with magnesium to produce sponge titanium. This sponge titanium is compacted and heated in a vacuum furnace to produce a titanium ingot. This ingot can be further processed to produce various titanium products, such as sheets, bars, wires, and tubes.

However, the Kroll Process has several disadvantages. Firstly, it is a costly process. The Kroll Process requires a significant amount of energy and uses expensive materials, such as chlorine and magnesium. Additionally, the process generates a significant amount of waste, including used chlorine and magnesium, which must be handled and disposed of safely.

Secondly, the Kroll Process is a multi-stage process that requires a considerable time investment. Each stage of the process must be carefully controlled to ensure the quality of the produced titanium. This can limit the ability to increase titanium production to meet demand.

Furthermore, the Kroll Process produces titanium in the form of ingots, which then need to be processed into the desired shape. This additional processing can introduce impurities into the titanium, which can affect its properties. Moreover, processing titanium ingots can be expensive and energy-intensive.

These challenges have limited the wider application of titanium alloys. Despite their attractive properties, the cost and complexity of titanium production have restricted its use to high-value applications where its unique properties are critical. However, advances in manufacturing technology, such as Additive Manufacturing, are opening up new possibilities for the use of titanium.

### 1.2.1  Titanium nowadays

The manufacturing of titanium today is a multi-stage process, each with its own challenges and associated costs. The process begins with the mining of titanium minerals, which are then processed to extract pure titanium. This titanium is then melted and refined to produce titanium alloys used in various industries.

The mining of titanium minerals itself is a costly and time-consuming process. Titanium minerals are found in the Earth's crust, but not in high concentrations. This means that a significant amount of mining and processing is required to extract a relatively small amount of titanium. Additionally, the mining process can have a significant impact on the environment, which can increase indirect costs associated with titanium production.

Once the titanium mineral has been extracted, it is processed to extract pure titanium. This is a complex process that involves a series of chemical reactions. These reactions can be challenging to control and require a significant amount of energy, which increases production costs.

After pure titanium has been extracted, it is melted and refined to produce titanium alloys. Melting titanium is challenging due to its high melting temperature and reactivity with oxygen. This means that titanium must be melted in a controlled environment to avoid contamination with oxygen. Titanium refining is also a complex process that requires precise control to ensure that the final alloy has the desired properties.

Despite these challenges, titanium alloys are highly valued for their unique properties, such as corrosion resistance and high strength-to-weight ratio. However, the costs and challenges associated with titanium production have limited its use to high-value applications where these properties are critical.

In summary, the manufacturing of titanium is a complex and costly process that presents several challenges. Despite the unique properties of titanium, these challenges have limited its wider application. However, advances in manufacturing technology, such as additive manufacturing, are opening up new possibilities for the use of titanium.

## 1.3  Additive Manufacturing

Additive Manufacturing (AM) is a set of technologies that construct three-dimensional objects layer by layer from a digital model. This approach contrasts with traditional manufacturing methods, which often involve the removal of material from a larger block. AM allows for greater design freedom, the ability to produce complex geometries, reduction of material waste, and customization.

AM has opened new possibilities for titanium and its alloys in various industries. In particular, AM can potentially alleviate some of the cost and manufacturing limitations associated with titanium alloys. For example, AM can enable the production of titanium parts with complex geometries that would be difficult or impossible to produce with traditional manufacturing methods. Additionally, AM can allow for the production of customized titanium parts, which can be useful in applications such as medicine, where custom implants may be required.

Common AM techniques include, Laser Powder Bed Fusion (LPBF), Directed Energy Deposition (DED), and Fused Deposition Modeling (FDM). Each of these techniques has its own advantages and disadvantages, and each is suitable for different applications.

### 1.3.1 Pros and cons of AM

Additive Manufacturing (AM), also known as 3D printing, offers several advantages compared to traditional manufacturing methods. One of the main benefits is the design freedom it provides. AM enables the creation of complex geometries and internal structures that would be difficult or even impossible to fabricate using conventional methods. Additionally, AM facilitates customization as it allows for the production of tailored parts without the need for costly tools or molds. This is particularly useful in fields such as medicine, where customized implants may be required.

Another significant advantage of AM is the reduction of waste. Unlike subtractive manufacturing methods that involve material removal from a larger block, AM adds material only where it is needed, minimizing waste generated during the process. Moreover, AM enables rapid prototyping, allowing for the quick creation of physical prototypes from digital models, thereby accelerating the design and development process.

AM also offers the ability to manufacture spare parts on-demand, reducing the need for maintaining large inventories of spare components. This can be especially beneficial in industries where immediate availability of spare parts is critical.

However, AM also comes with limitations and challenges. Firstly, production speed can be a limiting factor. While AM excels in producing customized parts and prototypes, it may be slower than traditional manufacturing methods for mass production applications. Thus, AM may be less suitable for certain large-scale production applications.

Additionally, the cost of materials used in AM can be higher compared to those used in traditional manufacturing methods. Especially with metal powders used in AM, special handling and storage requirements can further increase costs.

Size limitations are another consideration in AM. Although AM can produce complex geometries, there are constraints regarding the size of the parts that can be manufactured, particularly when compared to traditional methods.

Parts produced by AM often require post-processing steps to improve surface finish. This can increase both the time and cost of production. Moreover, ensuring consistency and repeatability can be challenging in AM, as variations may occur between parts due to factors such as material quality, machine calibration, and process parameters.

AM also involves specific design considerations. While it offers great design freedom, a different design approach is required. Designers must account for factors such as part orientation during printing and the necessary supports for overhanging geometries.

Furthermore, the cost of AM machinery can be significant. These machines are expensive to acquire and may require regular maintenance and calibration to ensure the quality of the produced parts.

Lastly, One of the biggest challenges in AM is ensuring the quality of printed parts. This means that defects are the most important issue being addressed and studied from the perspective of additive manufacturing. The process parameters of LPBF, such as laser power, scan speed, hatch spacing, hatch rotation, layer thickness, spot size, scan strategy, gas flow, part orientation, and baseplate material, are fully adjustable in an attempt to optimize the printing process. However, an incorrect selection of these values can result in a failed print, which will be discussed in more detail in the results section, as the first of the three prints conducted during this thesis was unsuccessful. The following are the most common defects encountered when using incorrect parameters for printing:

1. Layer Distortion or "Staircase Effect": Influenced by layer thickness and part orientation. The layer-by-layer process can lead to a step-like surface finish, especially for parts with inclined surfaces.

2. Lack of Fusion: Influenced by laser power, scan speed, and spot size. Insufficient energy input can lead to partially melted or unfused areas.

3. Balling Effect: Influenced by laser power, scan speed, and spot size. Instability in the melt pool can lead to spherical droplets of material adhering to the part surface, causing a poor surface finish.

4. Residual Stresses: Influenced by laser power, scan speed, layer thickness, and part orientation. Uneven heating and cooling can result in stresses that remain in the part after the process, causing warping or even part failure.

5. Keyhole Porosity: Influenced by laser power and scan speed. High energy input can create a deep, narrow melt pool (keyhole) that traps gas bubbles as it solidifies.

6. Gas Porosity: Influenced by the gas flow and material properties. The presence of gases in the powder or from the process environment can lead to pore formation during solidification.

7. Incomplete Melting or Solid State Sintering: Influenced by laser power, scan speed, and spot size. Insufficient laser energy can lead to weak bonding between particles.

8. Over-Melting: Influenced by laser power and scan speed. Excessive energy can lead to too much melting, causing deformation of the part or damage to previous layers.

9. Cracking: Influenced by laser power, scan speed, and material properties. Rapid cooling rates and high residual stresses can lead to cracking, especially in materials sensitive to thermal cycling.

10. Spatter: Influenced by laser power, scan speed, and gas flow. High energy or gas flow can lead to metal vaporization, causing small particles to be ejected from the melt pool, leading to a rough surface finish and potential loss of material.

11. Inclusions: Influenced by material properties and processing environment. Contamination of the powder or the process environment can result in foreign particles being embedded in the part.

### 1.3.2 Direct Energy Deposition

Directed Energy Deposition (DED) is another AM technique that can be used to fabricate titanium parts. In the DED process, an energy beam (such as a laser or an electron beam) is used to melt powder or wire material as it is deposited layer by layer. This allows for the construction of three-dimensional parts directly from a digital model. [**tshephe2022add**]

DED is particularly useful for the fabrication of large parts and for repair or addition applications to existing parts. Additionally, DED can enable the manufacturing of titanium parts with material gradients or customized properties, as different materials can be deposited and fused during the building process.

### 1.3.3 Fused deposition modeling

Fused Deposition Modeling (FDM) is an AM technique that uses a thermoplastic filament that is heated and extruded through a nozzle to build an object layer by layer. While FDM is commonly used with plastics, it can also be used with composite materials containing titanium powder.

FDM is a relatively inexpensive and user-friendly AM technique that can be used for a wide range of applications. However, titanium parts manufactured with FDM may not have the same properties as those produced with techniques such as PBF, as the material is a titanium composite rather than pure titanium. Nevertheless, FDM can be useful for prototyping and applications where the properties of pure titanium are not required.

### 1.3.4 Powder Bed Fusion

Laser Powder Bed Fusion (LPBF) uses a laser to melt and fuse metallic powder particles. LPBF does not require an inert gas environment, which can make the process more cost-effective and easier to implement.

LPBF is particularly suitable for manufacturing titanium parts due to its ability to produce parts with complex geometries and improved properties. Additionally, LPBF can enable the production of custom titanium parts, which can be useful in applications such as medicine, where custom implants may be required. The process begins by spreading a layer of metal powder on a retractable platform, which is then leveled using a powder cleaning system. The laser beam, guided by an expanded fiber laser, scanner mirrors, and a focusing lens, irradiates the powder particles, converting the energy into thermal energy and causing fusion. This energy is directed to specific locations on the powder bed to locally melt and solidify the metal powder.

1. Solid-State Sintering: This process occurs at temperatures below the material's melting point. The laser heats the powder particles, causing them to bond at their contact points through atomic diffusion, reducing the overall energy of the system by minimizing the surface area. Solid-state sintering primarily occurs during the initial stages of the LPBF process when the laser power is low or the scanning speed is high, resulting in a lower energy density. While this process helps to bind the powder particles together, it typically results in a porous structure with lower mechanical strength compared to fully melted parts.

2. Full Melting: This process occurs when the laser's energy is high enough to completely melt the powder particles. In full melting, the powder transforms into a liquid state, allowing it to flow and fill gaps before solidifying again. This leads to denser parts with higher mechanical strength, as the material solidifies into a near-fully dense, continuous piece.
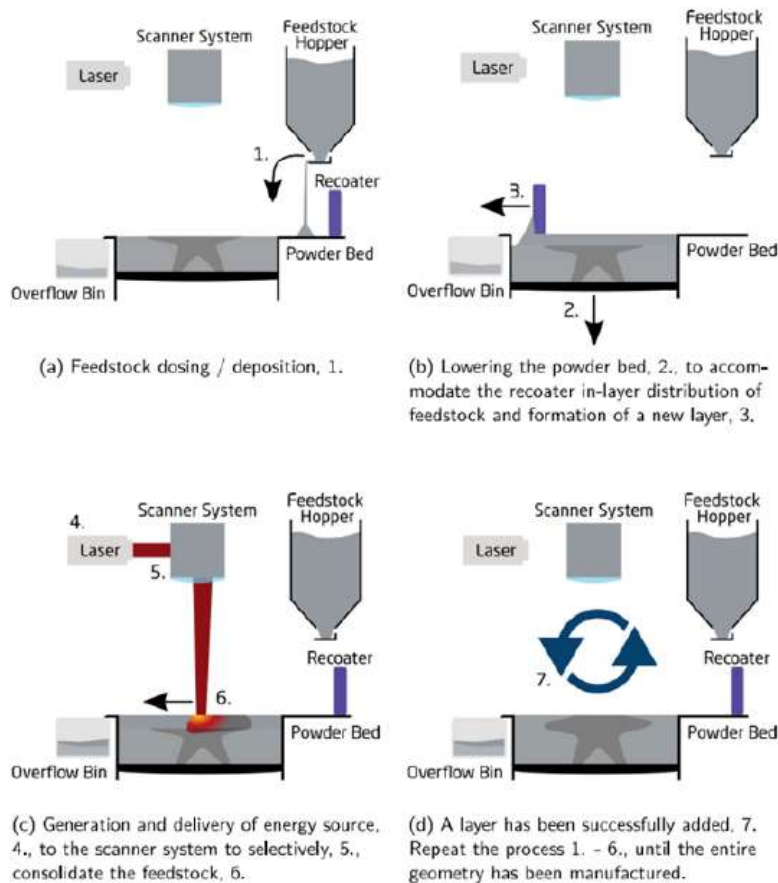
(a) Feedstock dosing / deposition, 1.

(b) Lowering the powder bed, 2., to accommodate the recoater in-layer distribution of feedstock and formation of a new layer, 3.

(c) Generation and delivery of energy source, 4., to the scanner system to selectively, 5., consolidate the feedstock, 6.

(d) A layer has been successfully added, 7. Repeat the process 1. – 6., until the entire geometry has been manufactured.

Figure 1.1: LPBF method [2]

In LPBF, the overall goal is usually to achieve full melting to create a solid and fully dense part. However, the process must be carefully controlled, as excessive energy input can lead to undesirable effects such as keyhole formation, spatter, and thermal stresses. Balancing the right process parameters such as laser power, scan speed, hatch spacing, layer thickness, and others is crucial to ensure a successful build.

After each layer is completed, the build platform is lowered by an amount equivalent to the layer thickness, typically 20 to 30 μm. A new layer of powder is spread, and the process is repeated until the final part is formed. The entire process takes place within a build chamber filled with inert gas, usually argon, to prevent oxidation. It is also important to note that this is where the hatch orientation is applied. Hatch orientation is a critical process parameter that significantly influences the characteristics of the resulting product. Specifically, a rotation of 67 degrees is applied to the hatch orientation of each subsequent layer. This rotation pattern is employed to optimize laser energy usage and enhance manufacturing productivity.

Furthermore, this hatch orientation strategy plays a pivotal role in regulating heat distribution across the build, which subsequently affects cooling and solidification rates, and ultimately, the microstructure and physical properties of the final product. By consistently applying a 67-degree rotation to the hatch orientation, the material's properties are uniformly distributed in all directions throughout the layers, reducing anisotropy and improving structural integrity. This approach also helps mitigate the formation of defects such as porosity and cracking, ultimately contributing to a superior surface finish in the final

Effect of atmosphere during additive manufacturing on the microstructure of Ti64

product. Therefore, hatch orientation is a vital aspect to be considered in additive manufacturing, with direct implications for product quality.

The general workflow of the entire process includes the preprocessing, processing, and postprocessing stages. In the preprocessing stage, a 3D model is created and converted into G-code, a programming language that instructs the machine on movements, fusion, and layering of the material. A specific job file for additive manufacturing is prepared, containing all the essential settings and parameters for the 3D printing process. In the processing stage, the feedstock, usually in the form of metal powder, is consolidated layer by layer to form the desired part according to the instructions in the G-code. In the postprocessing stage, the part is carefully removed from the build platform using a bandsaw or other means. The part then undergoes finishing processes to improve its surface finish and dimensional accuracy. Finally, verification and validation are performed to ensure that the part meets the required specifications and performs its intended function correctly.

Understanding the fundamental concepts of LPBF and discussing the process parameters and other phenomena that influence the resulting product are essential to predict the outcomes of the experimental phase and determine the goals and experimental settings of this thesis. Those concepts and parameters are:

1. Laser Power: The amount of energy the laser can deliver, typically measured in Watts.

2. Scan Speed or Laser Speed: The speed at which the laser moves across the powder bed.

3. Hatch Spacing or Hatch Distance: The distance between adjacent scan lines within a single layer.

4. Hatch Rotation: The angle at which the hatch pattern is rotated between subsequent layers.

5. Layer Thickness: The thickness of each layer of powder that is spread before the laser scans it.

6. Spot Size: The diameter of the laser beam when it hits the powder bed.

7. Scan Strategy or Scan Pattern: The path followed by the laser during the process.

8. Gas Flow: The flow of inert gas in the process chamber.

9. Part Orientation: The direction in which the part is built.

10. Baseplate material: The material of the baseplate.

## 1.4   Additive Manufacturing titanium

Laser Powder Bed Fusion (LPBF) is considered one of the best techniques for Additive Manufacturing (AM) of titanium for several reasons. First, LPBF can produce high-density parts with superior mechanical properties compared to other AM methods, making it ideal for applications where strength and durability are critical, such as aerospace or medical implant manufacturing. Second, LPBF offers design flexibility, enabling the production of complex geometries that would be difficult or impossible to achieve with traditional manufacturing methods. This includes intricate internal structures like cooling channels in aerospace engine components or porous structures in medical implants for better integration with surrounding tissue. Third, LPBF is an additive process, which means it uses

only the necessary material to form the part, resulting in more efficient material utilization, particularly valuable when working with expensive materials like titanium. Lastly, LPBF allows for precise control of the manufacturing process, including laser power, scanning speed, scanning strategy, and processing atmosphere, enabling process optimization to achieve desired part properties.

Within the LPBF process, the effects of different parameters, especially the atmosphere, have been investigated for both **CP-Ti and Ti64**. In the study focused on Ti64 fabrication with an inert atmosphere [3], a laser complex for direct metal deposition (CDLD) was utilized, employing the LS-5 fiber laser, along with various components such as a robot manipulator and a pan-tilt positioner. X-ray diffraction (XRD) analysis was conducted using a Bruker Advance D8 diffractometer, revealing the presence of thin acicular α-phases in the as-deposited state and the absence of the β phase. The microstructure analysis demonstrated the formation of the α + α'-phase resulting from rapid cooling from the β-phase zone.
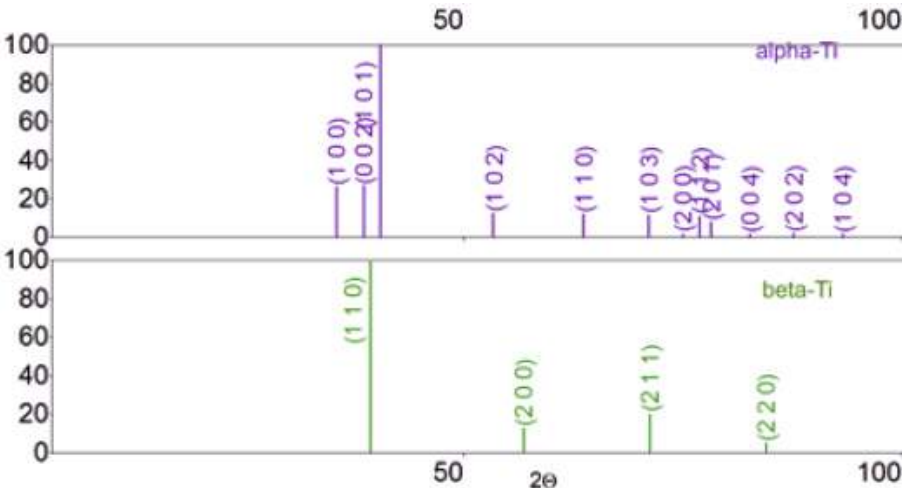


Figure 1.2: Ti64 XRD peaks [3]
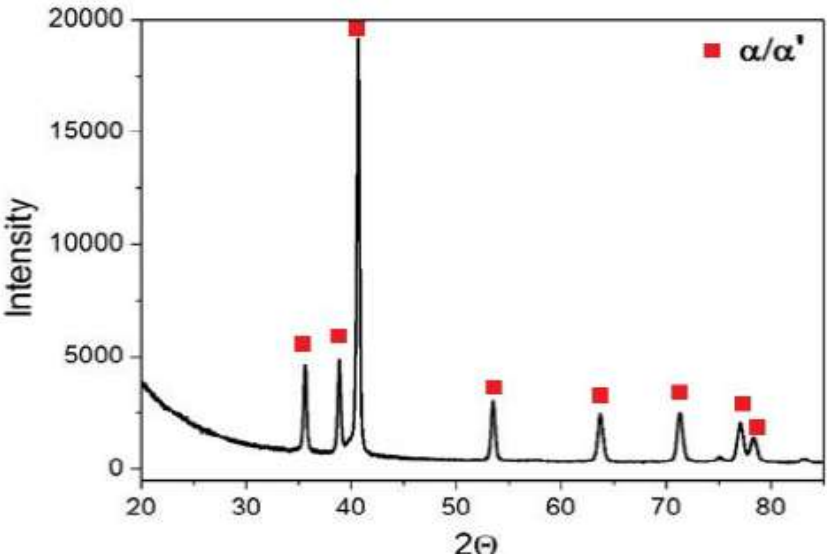


Figure 1.3: Ti64 printed with LPBF example peaks [3]

Effect of atmosphere during additive manufacturing on the microstructure of Ti64

In the investigation of a reactive atmosphere for CP-Ti [4], LPBF was employed to print CP-Ti components using Ar-N2 gas mixtures with varying N2 fractions. The aim was to identify the most efficient nitrogen concentration for achieving increased hardness without sacrificing ductility. The study provided insights into the use of a reactive atmosphere in LPBF for pure titanium fabrication, highlighting the potential for optimizing nitrogen concentration to enhance material properties. The presence of a reactive atmosphere, particularly Ar-N2 mixtures, was found to promote solid solution strengthening and exhibited an influence on the microstructure, phase evolution, and defects within the printed samples.
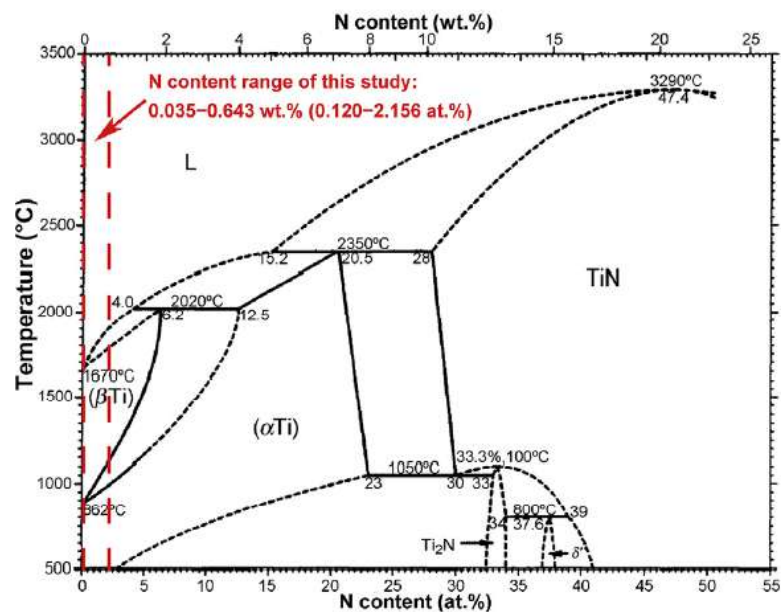


Figure 1.4: Ti-N phase diagram [4]

For the deposition of titanium nitride films [5], the direct current (DC) reactive magnetron sputtering technique was employed, utilizing different nitrogen fractions. The resulting films underwent extensive characterization, including thickness determination through grazing incidence X-ray reflectometry (GIXR) and crystal structure analysis using XRD. The incorporation of nitrogen led to the transformation of titanium from the α-Ti phase to the δ-TiN phase. Surface roughness decreased with increasing nitrogen content, and films with TiN(200) orientation exhibited a smoother surface compared to those with TiN(111) orientation.
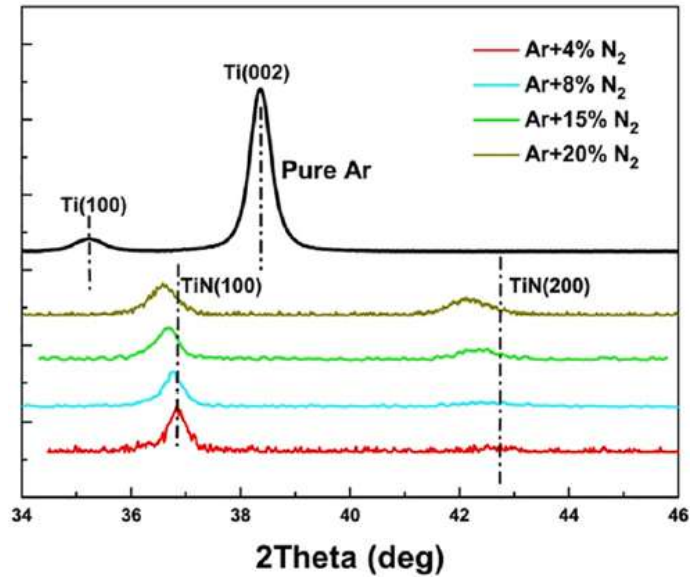
Figure 1.5: TiN peaks in XRD [5]

# 2 methodology

For the implementation of the experimental part of this thesis, first, the two prints were made using the open printers located in building 421 at DTU. Once the prints were completed, the samples were cut to separate them from the printing plate in order to begin the data analysis processes. These processes included light microscope (LOM) and X-ray diffraction (XRD). For LOM, the following processes were carried out: embedding, grinding, polishing, and etching. As for the XRD tests, the samples were placed on the plate and inside the machine, and then the appropriate parameters were introduced to carry out the test.

## 2.1 Printing

As this thesis revolves around the LPBF technique, it will focus on the use of LPBF (Laser Powder Bed Fusion) from DTU's Open Architecture see Figure 2.1. To perform the prints, common Ti6Al4V powder was used, which was filtered multiple times to prevent the presence of powder elements larger than 15 – 45 micrometers, which could cause problems or impurities in the print. Once filtered, it was stored in a material cartridge and loaded into the printer.



Figure 2.1: Open source DTU printer

The geometry of the cubes to be printed was designed, consisting of 8 cubes of 6x6x6 mm (216 mm$^3$) arranged in the shape of a square, with the center hollowed out to minimize the possibility of material traces detaching from one cube to another during printing and to achieve the purest possible print. Afterward, the code to be followed by the printer for the printing process was generated, including the movements of the laser, its power, and the scanning speed for each cube. During the printing, the parameters remained unchanged. The difference between the two prints is that the first one was performed in a pure Ar atmosphere, while the second one was done using a pre-mixture of Ar with 10% $N_2$, supplied by AVA. The different parameters used in the printings were:

| Power (W) | Speed (mm/s) | Hatch (mm) | Layer (mm) | VED (J/mm³) | Sample number |
|---|---|---|---|---|---|
| 250 | 500 | 0.1 | 0.05 | 100 | 1 |
| 250 | 1200 | 0.1 | 0.05 | 41.67 | 2 |
| 250 | 1100 | 0.1 | 0.05 | 45.45 | 3 |
| 250 | 900 | 0.1 | 0.05 | 55.56 | 4 |
| 250 | 800 | 0.1 | 0.05 | 62.5 | 5 |
| 250 | 700 | 0.1 | 0.05 | 71.43 | 6 |
| 250 | 600 | 0.1 | 0.05 | 83.33 | 7 |
| 250 | 1500 | 0.1 | 0.05 | 33.33 | 8 |

Table 2.1: Parameters and Sample Numbers

It should be noted that there were actually three printings but the first one, was unsuccessful because the printing plate was made of steel, which caused delamination and spalling but this failed print is not going to be studied in this thesis.

## 2.2 Samples preparation and characterization

The sample preparation and characterization part of the methodology involved several techniques and instruments. This included the cutting process using a radial cutter, the LOM (Light Optical Microscope) analysis, and the XRD (X-ray Diffraction) analysis using a Bruker D8 theta/theta goniometer. Each technique had specific steps and parameters to ensure accurate and reliable results. The cutting process involved separating the samples from the printing plate and achieving the desired surface. LOM analysis involved embedding, grinding, polishing, and etching the samples before microscopic examination. The XRD analysis utilized a goniometer and X-ray source to determine the crystallographic structure of the samples. These techniques and instruments played a crucial role in the subsequent data analysis and interpretation.

### 2.2.1 Cutting

For the cutting process, with the accustom 50 from Stuers a radial cutter was used. The cutting process was performed twice for each piece: first to separate each sample from the printing plate and second to achieve the desired surface for subsequent testing. Each cutting process involved three steps. The first step was placing the samples in the machine, followed by setting the cutting reference and parameters, and finally, the actual cutting process.
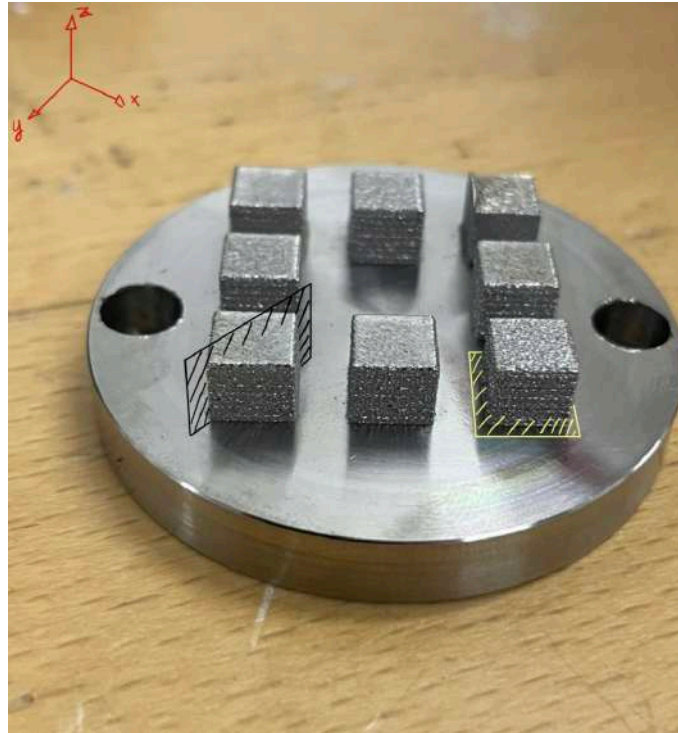
Figure 2.2: Plane description for cutting

For the first cut, the procedure was to align the printing plate parallel to the cutting wheel, then bring the samples as close as possible to the wheel to position the cutting reference. Subsequently, the cutting parameters were programmed, including force, speed, wheel revolutions, cutting direction, and length. The values used were 300N, 0.01mm/s, 3000rpm, a cutting depth of 4.5mm, and a length of 30mm, ensuring the cutting of all the samples. Before starting the cut, it is important to visually inspect for any potential issues such as the cutting of the printing plate or any interference between the plate and the base of the cutting wheel. Once verified, the cutting process was initiated. This cut was following the yellow plane in figure 2.2.

The procedure for the second cut was almost identical, with the only difference being the positioning of the sample at an angle of approximately 45 degrees. The objective was to leave the interior surface of the sample as the cutting surface to analyze the layers of the sample. Therefore, the only parameter that changed was the absence of cutting depth. The cut was performed by moving 7mm in the Y direction. A new reference position was set by placing the wheel as close as possible to the sample without touching it, positioned at the height closest to the arms holding the sample. This cut was following the black plane in figure 2.2.

### 2.2.2 LOM
To perform the LOM technique, the samples had to be prepared before placing them under the microscope. The following procedures were carried out on the samples: embedding, grinding, polishing, and etching. Once these steps were completed, the samples were placed under the microscope.

### Embeding
To carry out the embedding, the *ProntoPress-20* machine (see Figure 2.3) and the isofast method were used. The sample is placed with the surface to be studied in contact with the machine's support, and then the isofast resin is applied on top.

Figure 2.3: ProntoPress-20 machine

**Grinding**

To carry out the grinding process, the *RotoForce-4* machine was used (see Figure 2.4). A 500 $\mu$m paper was placed, and the samples were manually positioned at a 45º angle with the resin to avoid sharp edges on the handled part and prevent the diamond from lifting or expelling the lubricant or water due to the presence of corners in the sample.


Figure 2.4: RotoForce-4

**Polishing**

To carry out the polishing, the *RotoForce-4* machine (see Figure 2.4) was used. The sample was polished several times with different papers to ensure the surface of the sample was in the correct condition to be placed under the LOM. These papers included 500, 1000, and 4000 grit, as well as a 3µm and OPS. The aim was to create scratches in all directions so that the light always entered the sample in the same way, preventing variations in the views due to the sample's angle.

**Etching**

To carry out the etching process, the Keller's method was employed. This technique is used to remove sharp edges or burrs on the surface of a material. It involves immersing the material in a suitable chemical solution or etchant that selectively dissolves or attacks the edges, resulting in a smoother and rounded edge.

For the Keller's method, the following solution was used: 190mL distilled water, 5ml nitric acid (65%), 3mL hydrochloric acid (32%), and 8mL hydrofluoric acid (5%).

The process was conducted as follows: once the solution was prepared, it was placed in

a plastic container. The sample was then picked up using tweezers and immersed in the solution for 15 seconds. After this time, the sample was rinsed under a faucet with water for one minute, followed by a thorough cleaning of all items involved in the process.

**LOM analysing**

To analyze the samples under the LOM (Light Optical Microscope), the *Zeiss Axio Zen 2 core* machine with the *axiocam 305 color* filter was used (see Figure 2.5). Each sample was examined under different zoom levels to identify specific characteristics of each sample, as well as common features shared by the samples within the same atmosphere, which varied according to the printing parameters. The goal was to identify similarities and differences between the two different printing atmospheres. Zoom levels of x5, x10, x20, x50, and x100 were used. With each zoom level, the sample was adjusted to search for the mentioned features, and once the relevant photos were taken, the next zoom level was used. It was important to refocus with each zoom level to achieve a clear image. For setting the parameters for the photos, *auto exposure*, *white balance* and *gamma function* were all set to auto, allowing the program to choose the appropriate parameters for each photo.



Figure 2.5: Zeiss Axio Zen 2 core machine

### 2.2.3  XRD

Before starting the XRD analysis, the samples were placed on a transparent glass plate, which served as a shield to prevent any interference caused by the metal clamp. Once the samples were positioned, the parameters for the analysis were set.

The X-ray Diffraction (XRD) analysis was conducted using a Bruker D8 theta/theta goniometer, as shown in Figure 2.6. The testing setup included an open Eulerian cradle. A copper (Cu) anode was used as the X-ray source. The wavelength employed in the XRD test was 1.5406 Å, with a wavelength ratio of 0.5.

The goniometer was configured with a radius of 380 mm for the experiment. In the incident beam path, a fixed divergence slit of 1.2 degrees and Soller slits set at 2 degrees were utilized. It is important to note that no monochromator was incorporated into the setup. The received beam path included Soller slits set at 2 degrees, an 18-degree fixed anti-scatter slit, and, notably, no analyzer.

The X-ray generator was operated at 40 kV and 40 mA. The sample was positioned in the X, Y, Z coordinates, and the measurement was initiated at a 2θ angle of 30.0001 degrees. The diffraction data was collected in a coupled mode, with a step size of 0.03036 degrees and a step time of 960 seconds.

Figure 2.6: Bruker D8 Theta/Theta Goniometer used for XRD analysis

# 3  Results

In this section, we present the results obtained from the analysis of the samples using Light Optical Microscopy (LOM) and X-ray Diffraction (XRD) techniques. By analyzing the same samples from both printing conditions, we aimed to compare the results and draw meaningful conclusions regarding the impact of the nitrogen atmosphere and scanning speed on the printing process. The scanning speed parameter was individually analyzed for each sample. By examining the influence of scanning speed on the printing process, we can gain insights into the relationship between print quality and printing parameters.

The LOM analysis focused on samples 1, 4, 6, and 8 (Table 2.1) from both printing conditions. We examined the influence of the nitrogen atmosphere by comparing each sample with its corresponding counterpart in the other printing condition. Additionally, we looked for overall similarities and differences between the two printing conditions. Furthermore, a first printing that ended up as a failed printing is going to be analysed in order to explain why it failed and what can be seen in the LOM.

The XRD analysis, on the other hand, focused on samples 2, 3 and 5 (Table 2.1) from both printing conditions, as well as sample 6 from the reactive atmosphere printing. We analyzed the results by comparing the samples within each printing condition and also compared one of the samples analyzed in LOM, sample 6 from the reactive atmosphere printing. This comparison provides a comprehensive understanding of the samples' characteristics under both analysis methods.

In the following subsections, we will present the results obtained from the LOM and XRD analyses in detail.

## 3.1  Light optical microscope LOM

In this section, there is going to be presented the results obtained from the Light Optical Microscopy (LOM) analysis of the samples. The LOM analysis focused on samples 1, 4, 6, and 8 from both printing conditions: printing without nitrogen atmosphere and printing with nitrogen atmosphere. It should be noted that all the pictures shown in the following subsections are going to be also in the appendix but in a bigger size so the pictures can be seen with better detail (Appendix B).

### 3.1.1 Sample 1


(a) Sample 1 Ti64 x5 magnification


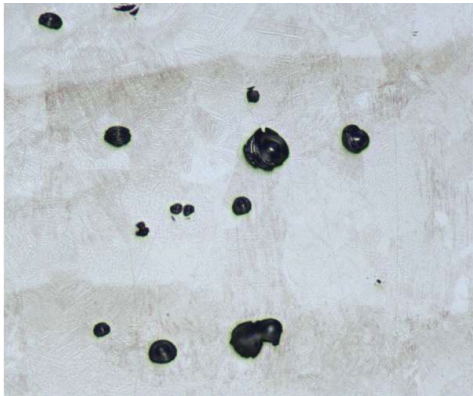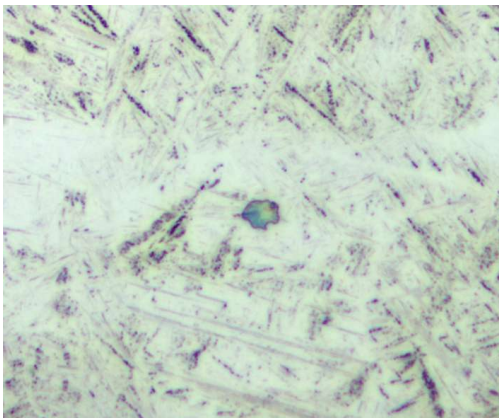(b) sample 1 Ti64 + N2 magnification x5


(c) sample 1 Ti64 x5 magnification


(d) sample 1 Ti64 + N2 magnification x5


(e) sample 1 Ti64 magnification x20


(f) sample 1 Ti64 + N2 magnification x10

Figure 3.1: Sample 1 (Table 2.1)

For sample 1, it is conducted a detailed examination of its surface morphology and microstructural features using LOM. The analysis revealed that in the first sample printed under the inert atmosphere, a significant number of large holes can be observed, likely due to the highest energy density used during the printing process. This is evident from the distinct layers that are visible on the surface, even at lower magnification. The dominance of the lighter-colored surface indicates the presence of the alpha martensitic structure.

Similarly, in the first sample printed under the Ar-N2 reactive atmosphere, a considerable number of large holes are also present, resulting from the very high energy density applied during printing. Detecting the individual layers at a 5x magnification is somewhat challenging, although they can be differentiated in various areas of the surface, particularly near the edges. Like the sample printed under the inert atmosphere, there is a clear dominance of the alpha martensitic structure. This can be attributed to the high cooling rate characteristic of the LPBF technique, which leads to the transformation of the beta phase into alpha martensite. Otherwise, a wavy-shaped structure would be evident.

### 3.1.2 Sample 4

(a) Sample 4 Ti64 x5 magnification

(b) sample 4 Ti64 + N2 magnification x5

(c) sample 4 Ti64 x100 magnification

(d) sample 4 Ti64 + N2 magnification x10 before etching

Figure 3.2: Sample 4 (Table 2.1)

When the fourth sample was analyzed, it was observed that the number of large holes was significantly reduced, with only small gas porosities remaining. The dominance of the alpha martensitic phase persisted, but in the melted regions, a wavy pattern that is expected from the beta phase could be seen, although it was not developed in the sample. This can be attributed to the creation of a large heat gradient, followed by rapid cooling, as mentioned earlier.

Similarly, in the analysis of the fourth sample from the printing with the reactive atmosphere, even fewer large holes were observed compared to the other printing. The whitish color of the alpha martensitic phase was more dominant in this sample. It was practically impossible to distinguish the individual layers in the picture.

Furthermore, the first image shows the surface before etching, where numerous points resembling surface porosities can be seen. These points are likely nitrides, which were subsequently removed using the chemical employed in the etching process.
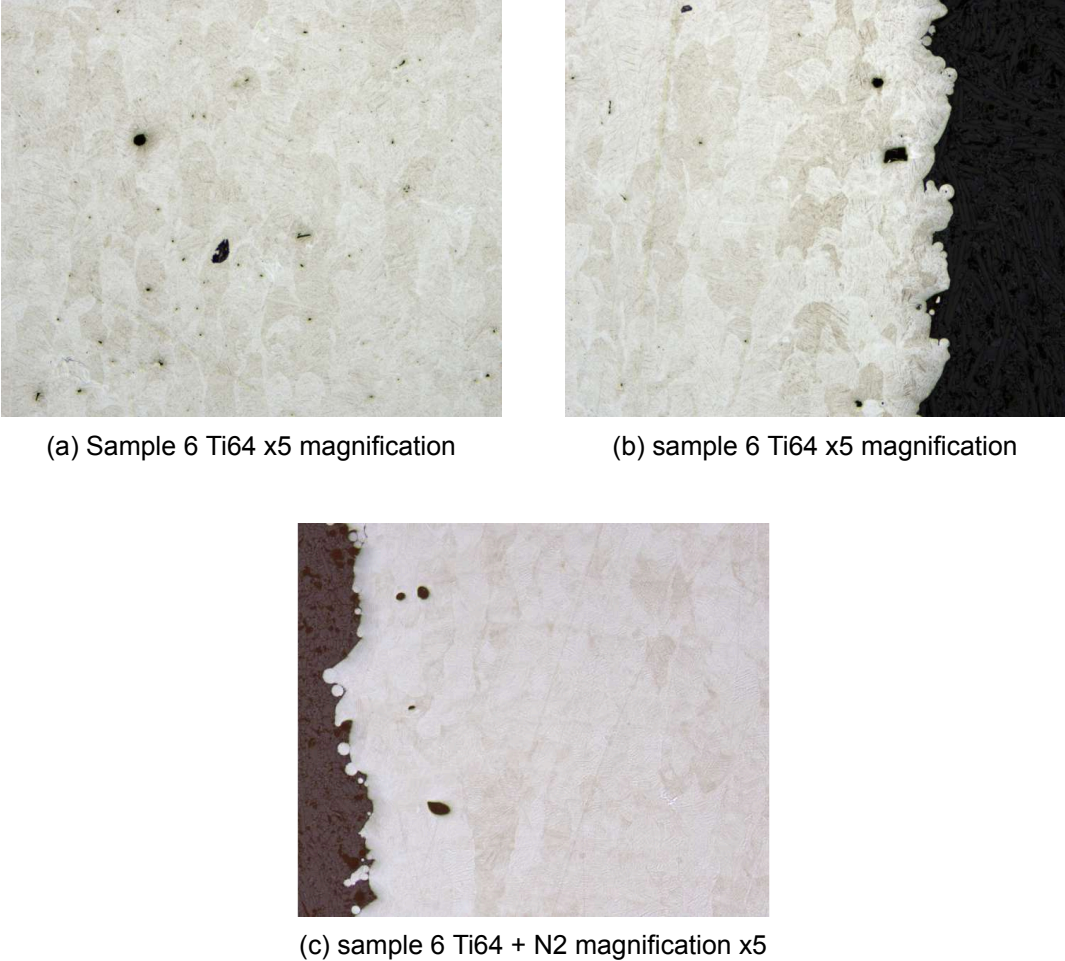
### 3.1.3 Sample 6



(a) Sample 6 Ti64 x5 magnification

(b) sample 6 Ti64 x5 magnification

(c) sample 6 Ti64 + N2 magnification x5

Figure 3.3: Sample 6 (Table 2.1)

The sixth sample shows similarities to the fourth sample in the inert atmosphere but with reduced porosity and an increased number of large holes. The whitish color from the alpha martensitic phase remains dominant.

Similarly, in the sixth sample of the reactive atmosphere printing, there is a significant decrease in porosity, almost none, and a reduction in the number of large holes compared to the other printing. The alpha martensitic phase is even more pronounced in this sample, and with the x5 zoom, the different layers on the surface can once again be observed.
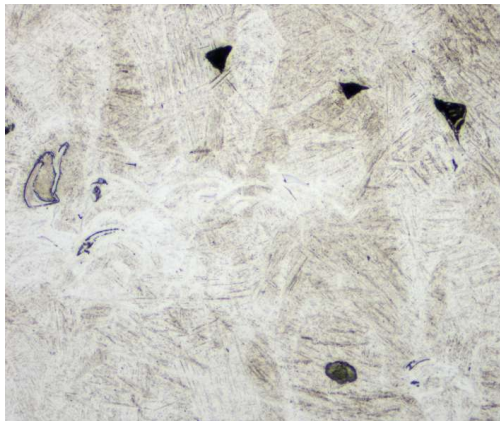
### 3.1.4  Sample 8
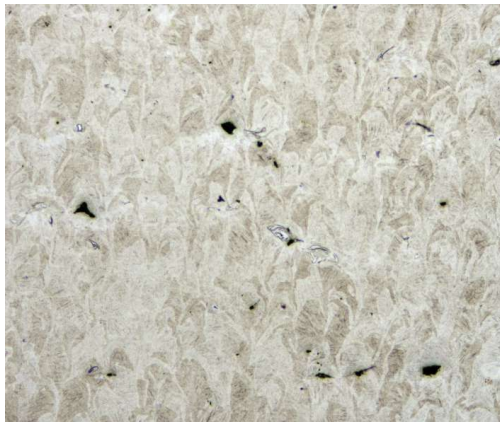

(a) Sample 8 Ti64 x5 magnification
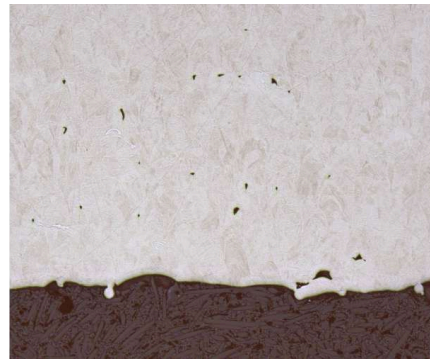

(b) sample 8 Ti64 + N2 magnification x5


(c) sample 8 Ti64 x20 magnification


(d) sample 8 Ti64 + N2 magnification x10 before etching

Figure 3.4: Sample 8 (Table 2.1)

The eighth sample had the highest energy density, and clear differences can be observed between this sample and the others. On one hand, a more wavy structure with reduced whitish color, which is expected on a Ti64 surface, can be seen. This sample exhibits more porosities and larger holes than the previous samples.

On the other hand, in the sample printed with the reactive atmosphere, it can be observed that the number of defects is significantly lower. Large holes are less common and smaller in size, and there are fewer small holes as well. The dominance of the whitish color from the alpha martensitic phase remains evident.

Furthermore, similar to sample 4, an image prior to the etching process is included, revealing even more porosities than in the other sample. These porosities translate into nitrides that are visually eliminated after applying the chemicals.

### 3.1.5  Comparison and discussion
after observing all the samples with each couple and in general it is been seen that:

1. In general, when using a reactive atmosphere, there is a reduction in the number and size of large holes and porosities compared to printing in an inert atmosphere.

2. The dominant phase observed in all samples, regardless of the atmosphere used,

is Alpha martensite, which does not align with the expected characteristics of Ti64 surfaces since it was expected to have some Beta phases, as it was explained this is because of the fast cooling rate while using LPBF. But the absence of Beta phases will be confirmed in the following sections, it can not be affirmed in the LOM since it is mostly impossible to see any Beta with this technique.

3. Increasing the energy density during printing correlates with a decrease in the presence of large holes and porosities, indicating improved print quality. Also, there were not seen any cracks in the surface. In the samples observed, the sample with the best printing quality was sample 4 in both the inert and the reactive atmosphere, which means that at a certain point, more energy density also means worse quality.

4. The possible presence of nitrides, identified as porosities in the pre-etching images, is significantly reduced after applying appropriate chemicals.

## 3.2 X-ray Diffraction XRD

In this section, there is going to be presented the results obtained from the X-ray diffraction (XRD) analysis of the samples. The XRD analysis focused on samples 2, 3, and 5 from both printing conditions and 6 from the reactive atmosphere printing (Table 2.1), this is due to the samples used in the LOM being unuseful and the other half of each sample was missing. this means that only reactive atmosphere sample 6 is used in both tests, so it can be compared. The results this time are going to be presented separately by the printing's atmosphere which means that in each subsection it is going to be shown individually the results obtained from the samples and then they are going to be compared with the other printing results afterward.

## 3.2.1 Inert atmosphere (Ar)



(a) sample 2
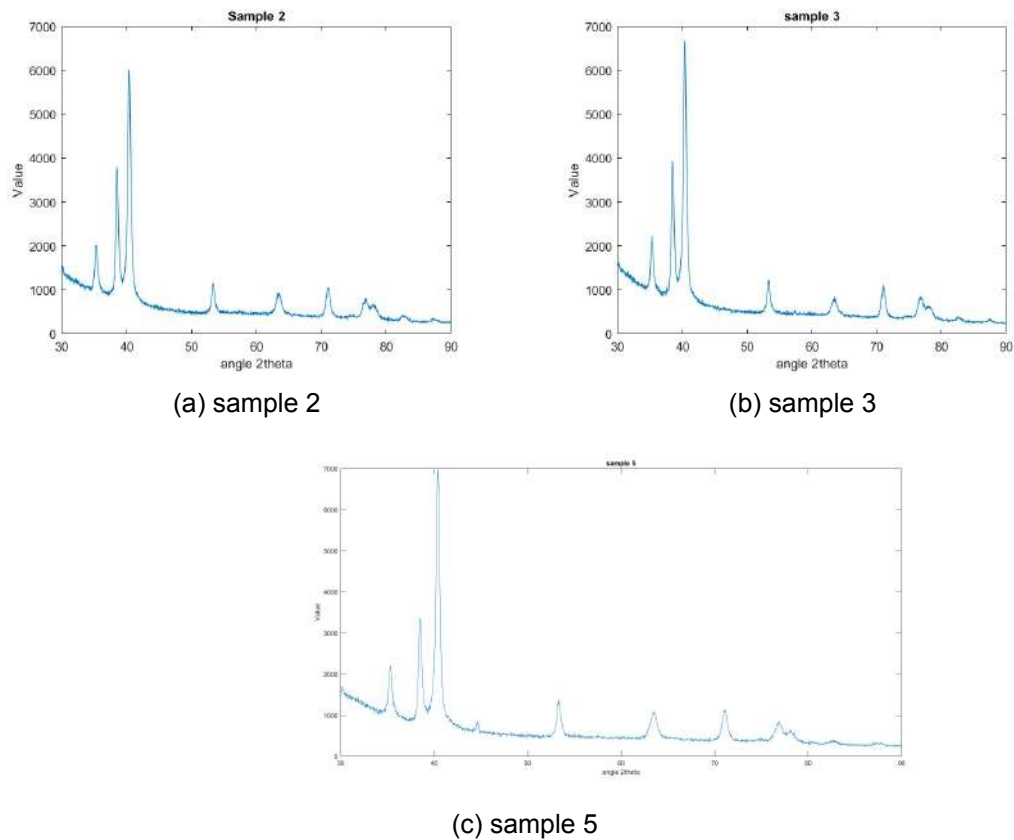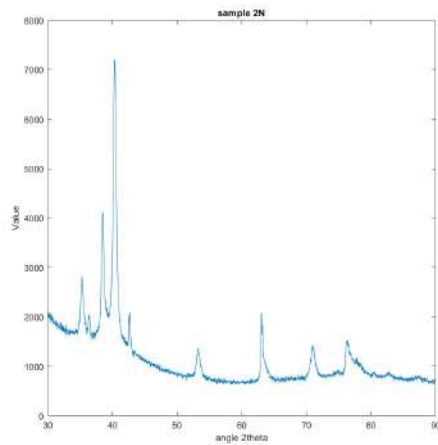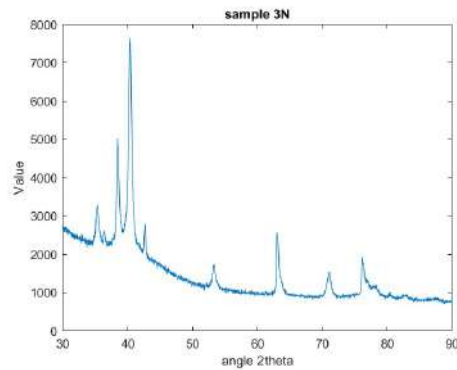


(b) sample 3



(c) sample 5

Figure 3.5: Inert atmosphere print

After examining the different XRD graphs obtained Figure 3.5, it is evident that only the Alpha phase and especially Alpha martensite is present, and no Beta phase is detected as observed in LOM. This can be attributed to the rapid heating and cooling process of LPBF, which leads to the transformation of the Beta phase into Alpha martensite. Comparing all the graphs from the different samples, they exhibit similar patterns, but the intensity of the peaks varies. However, in the case of sample 5, an additional peak appears right after the main peak, which does not match any known database. This anomaly could be attributed to a surface irregularity or an experimental artifact.
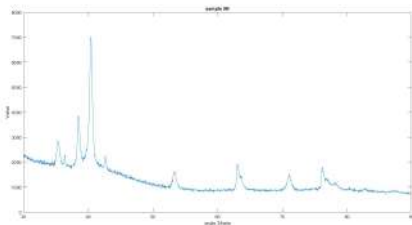
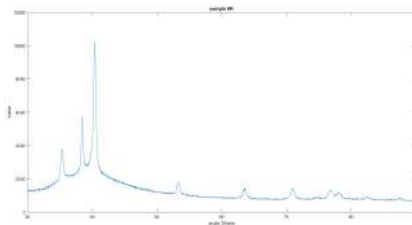### 3.2.2 Reactive atmosphere (Ar-N2)



(a) Sample 2 Ti64 + N2



(b) sample 3 Ti64 + N2



(c) sample 5 Ti64 + N2



(d) sample 6 Ti64 + N2

Figure 3.6: reactive atmosphere print

After examining the different XRD graphs obtained Figure 3.6, it is seen that only the Alpha phase and especially Alpha martensite is present, and no Beta phase is detected as observed in LOM. Also, it appears in each graphic two peaks which are titanium nitrides regarding to **??**, as it was also mentioned that before the etching those nitrides were shown in the LOM analysis. The only sample without those peaks is sample 6 (Figure 3.6d), this could be because it was the only one in which the surface under the analysis was the transversal one, like the one used for the LOM analysis samples, instead of the base of the cubes as it was done for the rest of the samples in the XRD.

### 3.2.3 Comparison and discussion

After comparing the XRD results obtained from the analysis of titanium printed with LPBF in a reactive Ar-N2 atmosphere (Figure 3.6) and in an inert Ar atmosphere (Figure 3.5), several observations can be made. In both cases, it is clear that the Alpha phase and particularly Alpha martensite, is present, while the Beta phase is not seen. This is consistent with the rapid heating and cooling process inherent to LPBF, which promotes the transformation of the Beta phase Alpha martensite.

In the XRD graphs for the samples printed in the reactive Ar-N2 atmosphere, two additional peaks are noticeable, which correspond to titanium nitrides as indicated in Figure 1.5. This finding aligns with the previous observation made during the LOM analysis, where the presence of these nitrides was noted. It is worth mentioning that these peaks are present in all the XRD graphs, except for sample 6 (Figure 3.6d). The absence of these peaks in sample 6 can be attributed to A higher energy density, which would elimi-

nate the nitrides, contradicts the results obtained in the LOM, where what appeared to be nitrides were present on the surface before etching (see Figure 3.4d). Therefore, it cannot be conclusively stated that what is visible in the image is indeed nitrides or if there was an error in sample 6. Further testing should be conducted on this sample to confirm. Turning to the XRD graphs for the samples printed in the inert Ar atmosphere, similar observations can be made regarding the presence of only the Alpha phase and predominantly Alpha martensite. The absence of the Beta phase aligns with the LPBF process's rapid heating and cooling characteristics. Comparing all the XRD graphs, they exhibit similar patterns, indicating the consistent presence of the Alpha phase. However, sample 5 shows an additional peak following the main peak, which does not correspond to any known database reference. This peculiar finding could be attributed to surface irregularities or potential experimental artifacts that require further investigation.

In summary, the XRD analysis of titanium printed using LPBF reveals the dominance of the Alpha phase and particularly Alpha martensite, regardless of the atmosphere used during printing. The presence of titanium nitride peaks in the XRD graphs for the samples printed in the reactive Ar-N2 atmosphere confirms the previous observations made during the LOM analysis. The absence of these peaks in sample 6 indicates the influence of the surface analyzed. Additionally, the detection of an unaccounted peak in sample 5 highlights the need for additional studies to understand its origin and significance.

Effect of atmosphere during additive manufacturing on the microstructure of Ti64

# 4 Conclusions

## 4.1 future work

In future work, it is recommended to conduct additional investigations to further enhance the understanding of the effects of reactive atmospheres in LPBF of titanium alloys. SEM and EDS analysis can provide valuable insights into the microstructure, phase composition, and the influence of intermetallic structures within the samples. These analyses would shed light on the mechanisms and characteristics associated with the reactive atmosphere.

To address the observed defects and improve sample quality, further research can be focused on optimizing the process parameters. Fine-tuning laser power, scanning speed, and powder feed rate can help minimize surface irregularities and enhance the overall homogeneity of the printed samples.

Furthermore, it is crucial to conduct a comprehensive suite of tests to evaluate the mechanical properties, chemical composition, and other relevant characteristics of the fabricated titanium components. Hardness testing and chemical composition analysis would provide valuable information on the material's strength, ductility, and elemental composition.

By addressing these aspects in future research, a more comprehensive understanding of the impact of reactive atmospheres on the additive manufacturing of titanium alloys can be achieved. This knowledge will contribute to the advancement of LPBF processes and the production of high-quality titanium components.

## 4.2 Discussion and conclusion

In conclusion, this study has successfully achieved its main objectives of fabricating titanium samples using Laser Powder Bed Fusion (LPBF) in both an inert atmosphere and a reactive Ar-N2 atmosphere. The influence of the reactive atmosphere on the microstructure and phase composition of Ti6Al4V additive manufacturing has been analyzed. Despite time constraints, the experimental phase of the project can be considered a success, laying the foundation for future investigations.

The analysis of X-ray Diffraction (XRD) results revealed several important observations. In both printing conditions, the dominant phase observed in the samples was Alpha martensite, contrary to the expected presence of Beta phases. This can be attributed to the rapid heating and cooling process inherent to LPBF, which promotes the transformation of Beta phase into Alpha martensite. It should be noted that the absence of Beta phases was confirmed by XRD analysis, as they were not detectable in any of the samples.

Comparing the XRD results between the samples printed in the reactive Ar-N2 atmosphere and the inert Ar atmosphere, similar patterns were observed, indicating the consistent presence of the Alpha phase. However, samples printed in the reactive atmosphere exhibited two additional peaks corresponding to titanium nitrides, confirming the previous observations made during the optical microscopy analysis. Notably, sample 6 in the reactive atmosphere did not show these peaks, which may be attributed to factors such as the specific surface analyzed or potential experimental errors. Further testing on this sample is recommended to confirm the presence of nitrides.

Furthermore, the analysis of the samples revealed that an increase in energy density during printing correlated with a reduction in the presence of large holes and porosities, leading to improved print quality. The absence of cracks on the surface of the samples further supports the overall printing success. Among the samples observed, sample 4 exhibited the best printing quality in both the inert and reactive atmospheres, indicating that there is an optimal energy density range for achieving high-quality prints.

The results also indicated that appropriate chemical treatment effectively reduced the presence of potential nitrides, initially identified as porosities in the pre-etching images. This highlights the importance of post-processing steps in obtaining accurate microstructural information.

Addressing the observed defects and enhancing sample quality should also be a priority for future research. Optimizing process parameters, such as laser power, scanning speed, and powder feed rate, can help minimize surface irregularities and improve sample homogeneity.

Overall, this study contributes to the understanding of the effects of reactive atmospheres in LPBF of titanium alloys. It opens up possibilities for further research in areas such as mechanical properties, chemical composition, and defect reduction strategies, which can ultimately enhance the overall quality and performance of additively manufactured titanium components. The student has successfully achieved the stated learning objectives of working independently, describing the principles of metal additive manufacturing, performing metallographic investigations, and critically evaluating acquired knowledge.

# bibliography

[1]   Thato Sharon Tshephe et al. "Additive manufacturing of titanium-based alloys - A review of methods, properties, challenges, and prospects". In: *Heliyon* 8 (2022), e09041.

[2]   S. A. Andersen. "Open Architecture Laser Power Bed Additive Manufacturing". PhD thesis. Technical University of Denmark, 2020.

[3]   O G Klimova-Korsmik et al. "Structure and properties of Ti-6Al-4V titanium alloy products obtained by direct laser deposition and subsequent heat treatment". In: *J. Phys.: Conf. Ser.* 1109 (2018), p. 012061.

[4]   D.W. Wang et al. "Selective laser melting under the reactive atmosphere: A convenient and efficient approach to fabricate ultrahigh strength commercially pure titanium without sacrificing ductility". In: *Materials Science & Engineering A* 762 (2019), p. 138078.

[5]   Runze Qi et al. "Evolution of chemical, structural, and mechanical properties of titanium nitride thin films deposited under different nitrogen partial pressure". In: *Results in Physics* 19 (2020), p. 103416.

Effect of atmosphere during additive manufacturing on the microstructure of Ti64

# A  instructions

## A.1  embeding

**Pre-use**
Before operating the ProntoPress-20 machine, the following steps were performed:

- Turn on the cooling water supply, ensuring a direct line connection.

- Power on the ProntoPress-20 machine, ensuring all necessary controls are functional.

- Close the tower of the machine to secure the workspace and prevent any interference.

- Select the isofast method from the available options.

- Apply an anti-stick agent to both surfaces of the samples.

### A.1.1  Usage

To carry out the embedding process using the ProntoPress-20 machine, the following steps were followed:

- Clean the specimens thoroughly to remove any contaminants.

- Place the specimens in a centered position on the support within the machine.

- Lower the tower of the ProntoPress-20 machine carefully to prepare for the embedding process.

- Close the tower securely to create an enclosed environment for embedding.

- Start the embedding process using the selected isofast method.

- Once the process is completed, turn off the ProntoPress-20 machine.

- Turn off the cooling water supply to conserve resources.

### A.1.2  Safety

Ensuring safety during the operation of the ProntoPress-20 machine is of utmost importance. The following safety precautions were observed:

- Avoid looking from above when the tower of the ProntoPress-20 machine descends to prevent potential hazards.

- Always switch off the cooling water supply after completing the embedding process to conserve resources and prevent unnecessary waste.

## A.2  polishing

### A.2.1  Pre-use

Before operating the machine, the following steps were performed:

1. Turn on the machine.

2. Turn on the water supply, filling it up to 3/4 of the total capacity.

3. Turn on the gas supply.

4. Put the sample holder in place.

## A.2.2  Usage

To use the machine, follow these steps:

1. Put water into the machine.

2. Place the 500-grit paper onto the machine's surface.

3. Move the head to the correct position, aligning the sample holder close to the edge of the paper.

4. Place the samples symmetrically.

5. Set the machine parameters for the samples and paper to rotate in the same direction. Set the force to 5N, the time to 3 minutes, and turn on the auto button for communication between the head and body of the machine.

6. Allow water to flow slowly for the 500-grit paper.

7. Repeat steps 2-6, using a 1000-grit paper and adjusting the water flow to a slower rate.

8. Repeat step 7, using a 4000-grit paper and reducing the water flow to just a few droplets.

9. Check if the sample and resin are on the same level.

10. Change to the Mol plate and use the 3µm diamond suspension with the appropriate oil-based lubricant for titanium. Adjust the parameters to 4 minutes and 10N.

11. Apply water to fill the pores of the neoprene disc, then apply a mix of OPS (Oxide Polishing Suspension) and water for 4 minutes with 5N force. Ensure the samples and plate rotate in opposite directions. Afterward, clean everything with water for 2 minutes.

## A.2.3  Safety

To ensure safety during the operation of the machine, the following precautions were observed:

• Make sure nothing is loose in the area.

• Avoid hitting anything in the lower part of the machine while centering the samples.

• Turn on the ventilation system.

• Stay near the machine during the polishing process.

• Use a kettle, safety glasses, and gloves for protection.
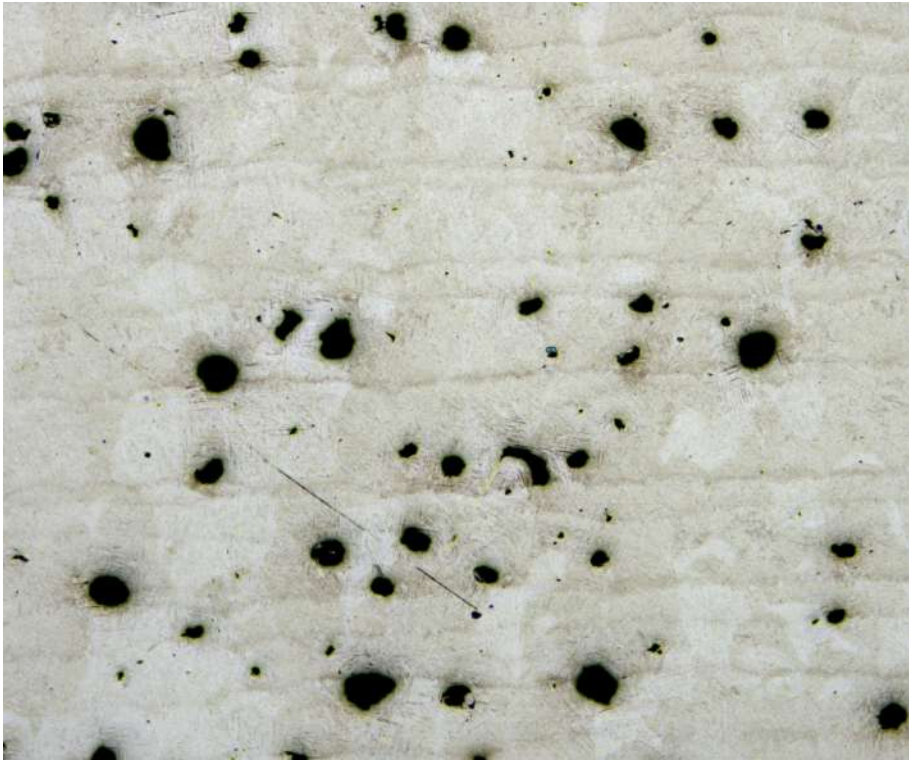
# B Pictures



Figure B.1: Sample 1 x5

Figure B.2: Sample 1 x5



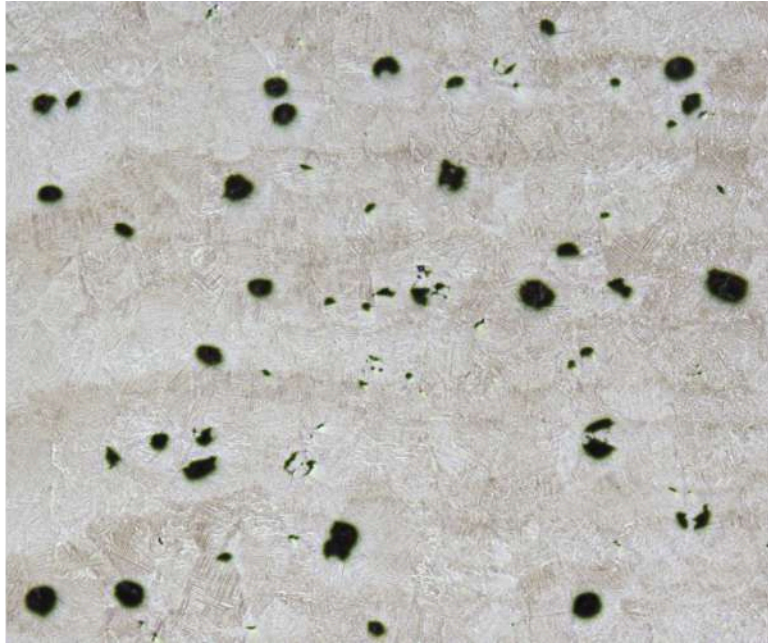Figure B.3: Sample 1 x20

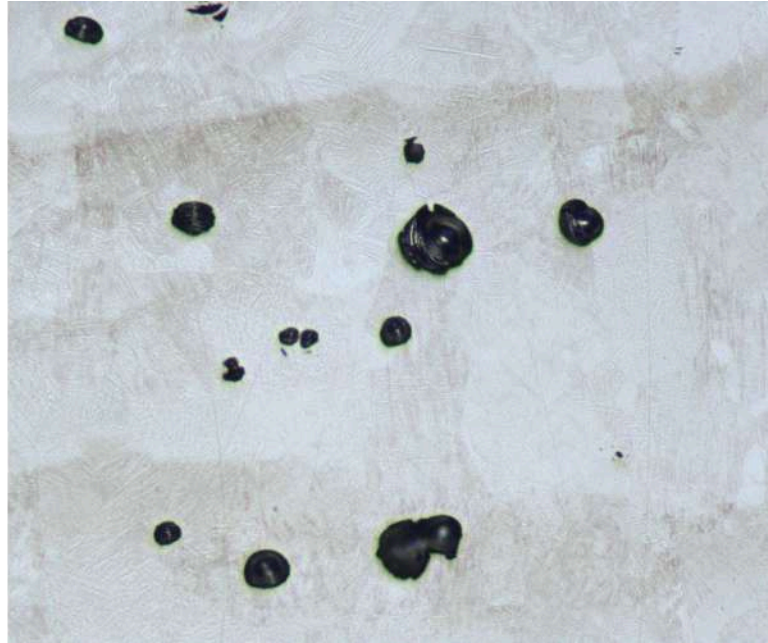Figure B.4: Sample 1N x5


Figure B.5: Sample 1N x5

Figure B.6: Sample 1N x10
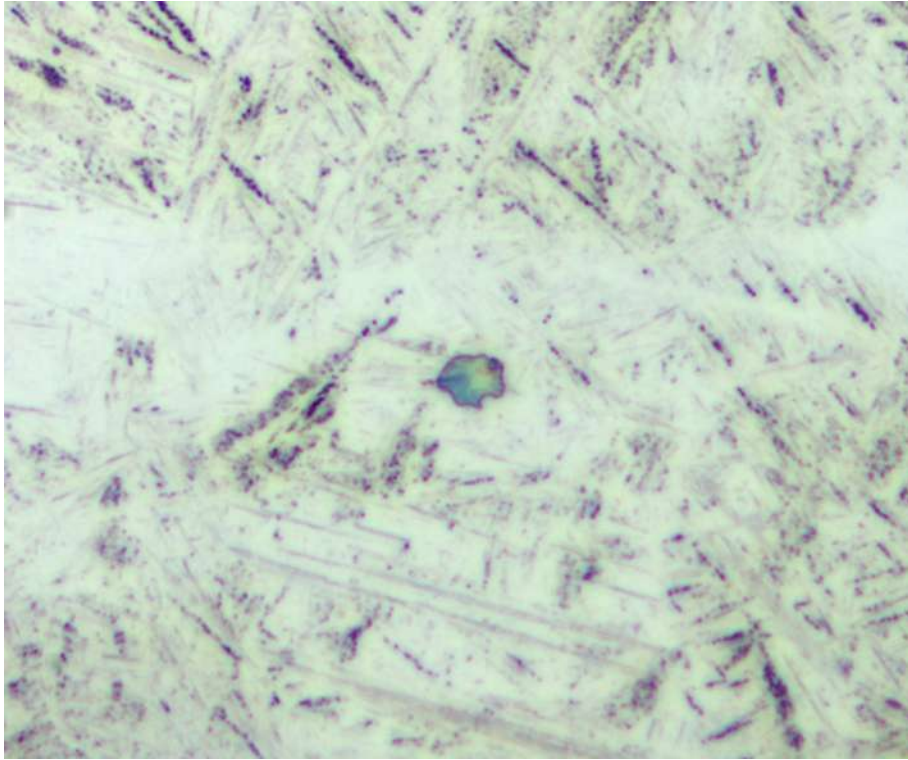


Figure B.7: Sample 4 x5

Figure B.8: Sample 4 x100
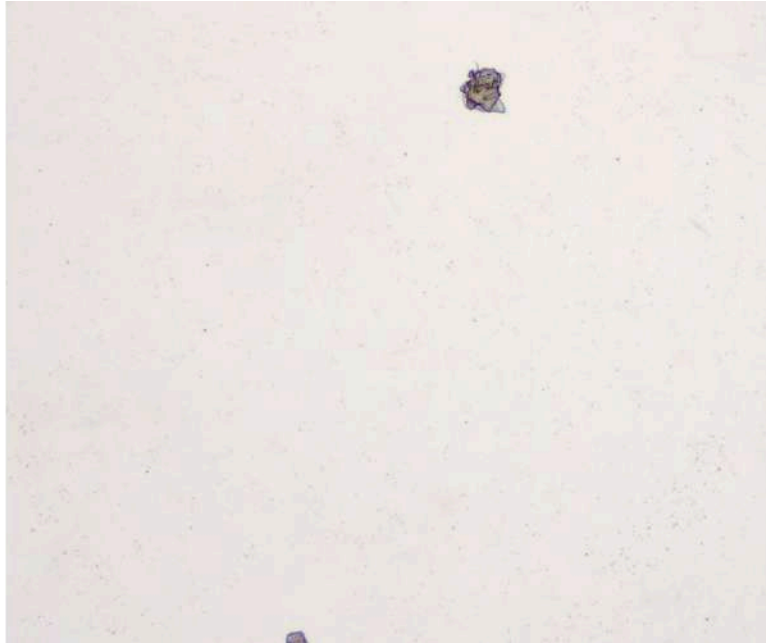


Figure B.9: Sample 4N x5

Effect of atmosphere during additive manufacturing on the microstructure of Ti64

Figure B.10: Sample 4N x10 before etching



Figure B.11: Sample 6 x5

Figure B.12: Sample 6 x5



Figure B.13: Sample 6N x5

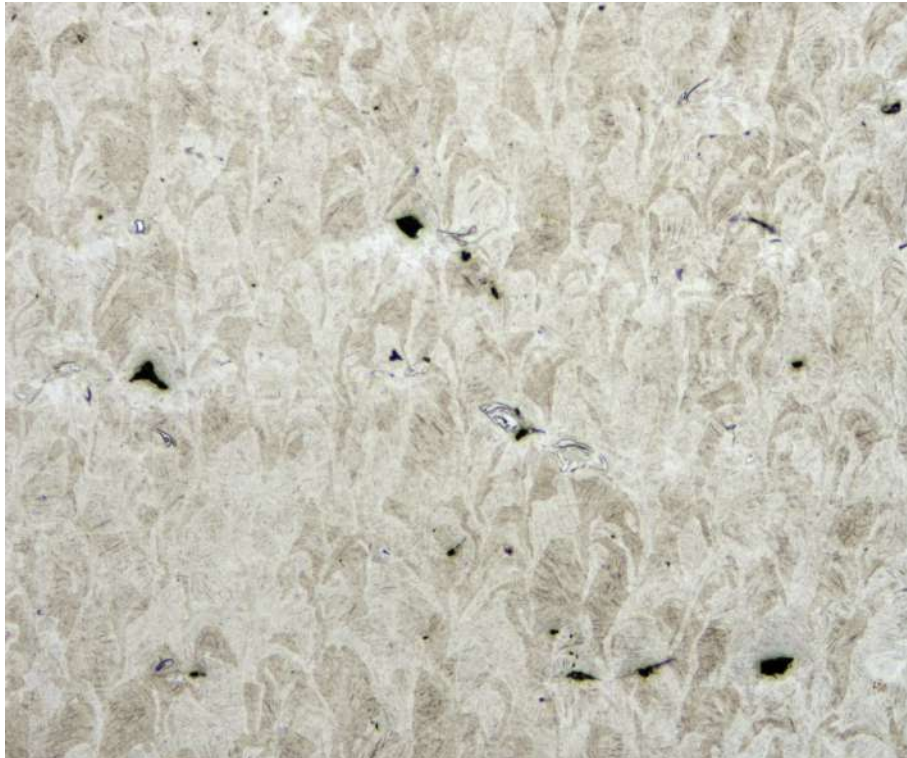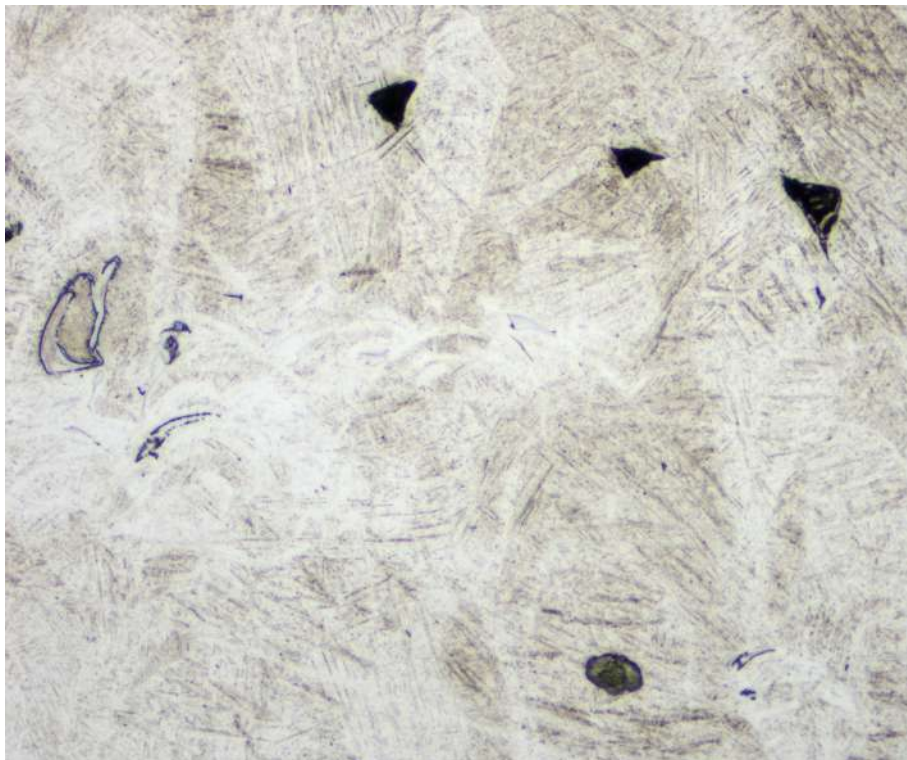Effect of atmosphere during additive manufacturing on the microstructure of Ti64

Figure B.14: Sample 8 x5



Figure B.15: Sample 8 x20
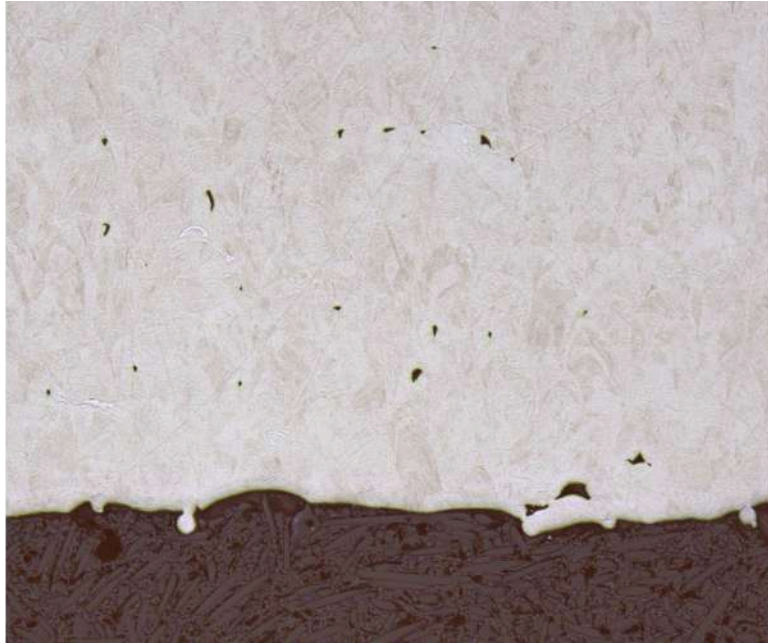
Figure B.16: Sample 8N x5



Figure B.17: Sample 8N x10 before etching

Effect of atmosphere during additive manufacturing on the microstructure of Ti64